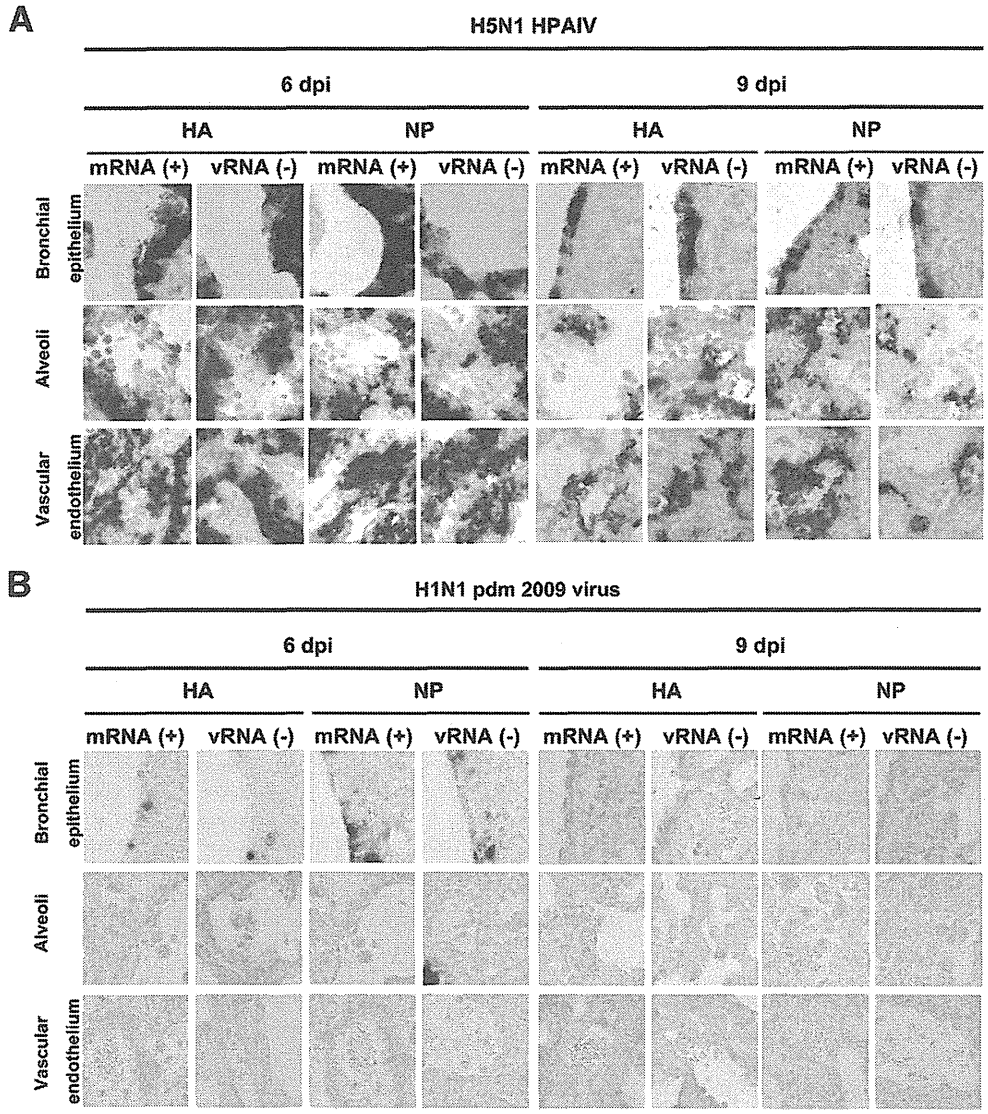

Figure 4 Detection of influenza virus RNA in the lungs of mice infected with H5N1 HPAIV or H1N1 pdm 2009 virus. **A** and **B**: *In situ* hybridization analyses were performed in H5N1 HPAIV-infected murine lung samples (**A**) or H1N1 pdm 2009 virus-infected murine lung samples (**B**) using DIG-labeled RNA probes specific for vRNA and mRNA. Representative figures at each time point (four mice per time point) are shown, with the three rows of images in both **A** and **B** corresponding to bronchial epithelium, alveoli, and vascular endothelium. Original magnification, ×630. dpi, days post-infection.

bronchiole, but rarely in pneumocytes, at 6 days after infection (Figure 4B). The H1N1 viral transcripts were not detected in the lung at 9 days after infection.

Proliferation of Macrophages after Infection with Influenza Viruses

A dual-staining technique was used to discriminate proliferating macrophages from residential macrophages in the alveoli of lung specimens from virus-infected mice. Cells that stained positive for both PCNA and a macrophage-specific marker (Iba1) ($PCNA^+/Iba1^+$) may be newly proliferating macrophages or may be derived from infiltrating monocytes. In mice infected with H5N1 HPAIV, images of dual-stained lung tissue revealed extensive proliferation of the macrophages, with progressively increasing numbers of macrophages seen starting from day 3 after infection (Figure 5A). This proliferation was confirmed by IHC scoring, achieving a mean IHC score of 4.0 (extensive positive cells) by day 9 after infection (Figure 5B). At that time, the proportion of $PCNA^+/Iba1^+$ cells against total $Iba1^+$ cells reached approximately 90% (Figure 5B). In mice infected with H1N1 pdm 2009 virus, proliferation of the macrophages in the alveoli also was observed after infection (Figure 5C). However, mean IHC scores remained ≤ 1.0 (rare positive cells) through day 9 after infection (Figure 5D). The proportion of $PCNA^+/Iba1^+$ cells was only approximately 30% (Figure 5D).

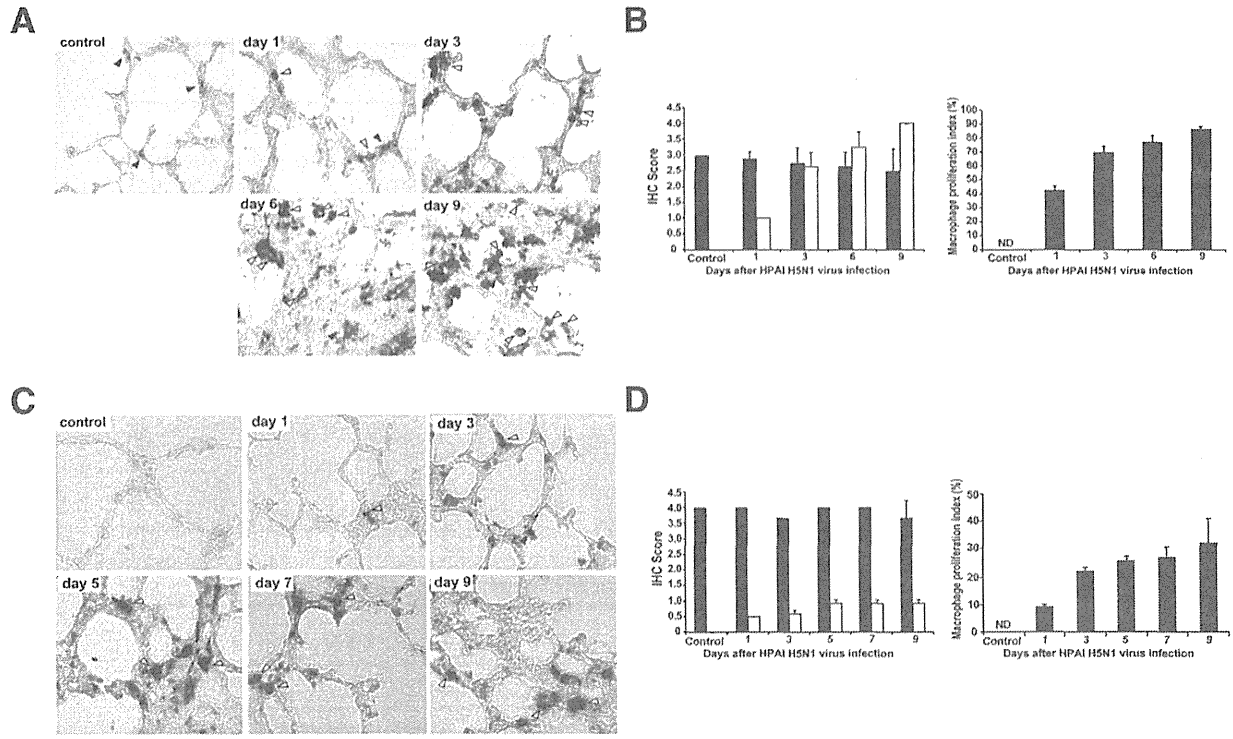

Figure 5 The proliferation of alveolar macrophages infected with H5N1 HPAIV or H1N1 pdm 2009 virus. Double immunostaining was performed for PCNA and alveolar macrophage-specific marker (Iba1) in mice infected with H5N1 HPAIV (**A** and **B**) or influenza A/H1N1 pdm 2009 virus (**C** and **D**). **White arrowheads**, proliferating alveolar macrophages ($PCNA^+/Iba1^+$); **black arrowheads**, resident alveolar macrophages ($PCNA^-/Iba1^+$). **B** and **D**: The cells with positive staining were counted in 10 randomly selected microscopic fields of individual animals, and mean IHC scores were calculated. Original magnifications: ×630 (**A** and **B**). Black bars indicate number of resident macrophages ($PCNA^-/Iba1^+$); white bars, number of newly proliferated macrophages ($PCNA^+/Iba1^+$). Proliferation index, defined as the number of proliferating macrophages ($PCNA^+/Iba1^+$) expressed as a percentage of total macrophage ($Iba1^+$) numbers. These observations were performed in three to four mice per time point. Data are shown as means ± SD. ND, not detected.

Proliferation of Type II Pneumocytes after Infection with Influenza Viruses

In parallel with the macrophage study previously performed, we used a dual-staining technique to discriminate proliferating type II pneumocytes (cells that stained positive for both PCNA and a pneumocyte-specific marker (SP-C; $PCNA^+/SP\text{-}C^+$) (Figure 6A) from indigenous type II pneumocytes ($PCNA^-/SP\text{-}C^+$) (Figure 6A). In mice infected with H5N1 HPAIV, proliferation of type II pneumocytes peaked at 6 days after infection and subsequently decreased (Figure 6B). Mean IHC scores were approximately 3.0 (common positive cells) and <1.0 at 6 and 9 days after infection, respectively. The proportion of $PCNA^+/SP\text{-}C^+$ cells reached approximately 60% at 6 days after infection (Figure 6B). In mice infected with H1N1 pdm 2009 virus, proliferation of type II pneumocytes also was observed (Figure 6C), although alveolar injuries were rarely seen in H&E-stained lung specimens (compare to the injuries shown in Figure 1D). Proliferation of type II pneumocytes progressively increased through 9 days after infection with H1N1 pdm 2009 virus, in contrast to the time course seen after infection with H5N1 HPAIV. IHC score and proportion of $PCNA^+/SP\text{-}C^+$ cells reached approximately 2.5 and >50%, respectively (Figure 6D).

Expression of Cytokines and Chemokines in the Lung Tissues after Infection with Influenza Virus

To analyze the immune responses of BALB/c mice after infection with H5N1 HAPIV or H1N1 pdm 2009 virus, we measured multiple cytokines and chemokines in lung homogenates (Figure 7). As shown in Figure 7A, expression levels of several proinflammatory cytokines were considerably higher in the lung of H5N1 HPAIV-infected mice than H1N1 2009 pdm virus-infected mice. Specifically, H5N1 HPAIV-infected mice exhibited the increase of IL-6 and IFN-γ 3 to 9 and 6 to 9 days after H5N1 HPAIV infection, respectively. IL-1β and TNF-α were considerably induced from 1 day after H5N1 HPAIV infection. In addition, macrophage-stimulating factors, including MCP-1, MIP-1α, and G-CSF, increased 6 to 9 days after H5N1 HPAIV infection (Figure 7B). These results were temporally consistent with massive infiltration of macrophages and progression of tissue damage.

Discussion

In this study, we showed that infection of mice with H5N1 HPAIV caused serious lung damage leading to DAD, with

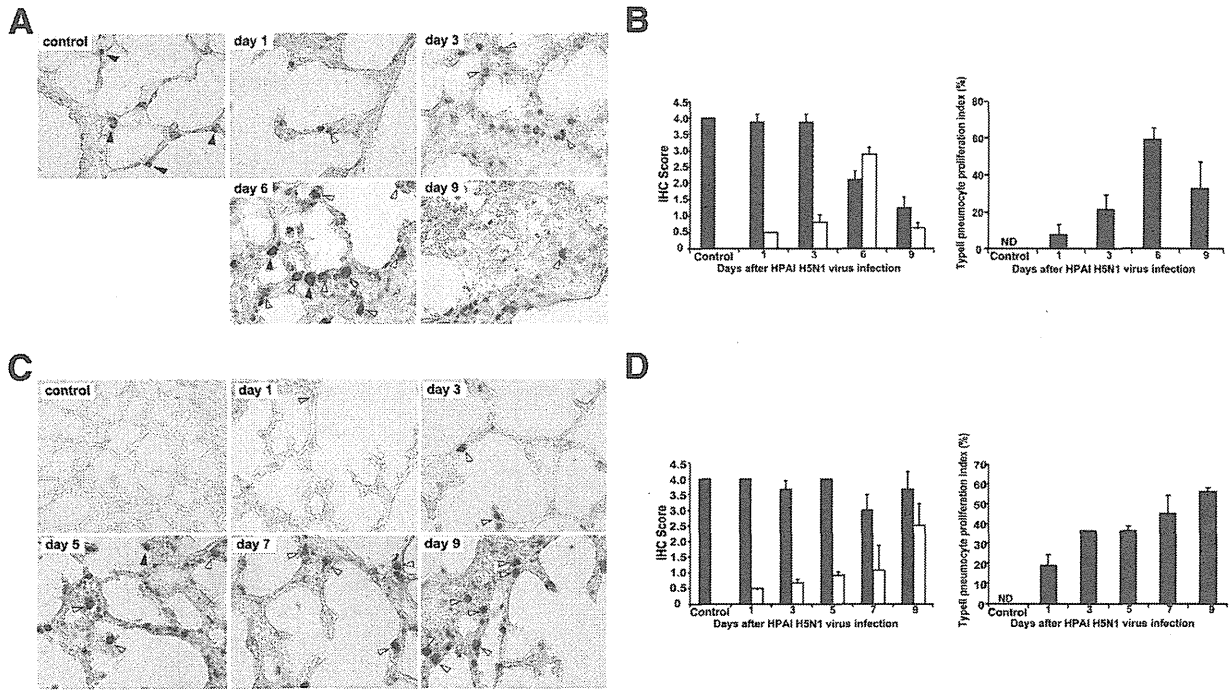

Figure 6 The proliferation of type II pneumocytes after infection with H5N1 HPAIV or H1N1 pdm 2009 virus. The proliferation of type II pneumocytes after infection with H5N1 HPAIV (**A** and **B**) or H1N1 pdm 2009 (**C** and **D**) was estimated. Double immunostaining was performed for PCNA and SP-C, a marker for type II pneumocytes. **White arrowheads** indicate proliferating type II pneumocytes ($PCNA^+/SP\text{-}C^+$); **black arrowheads**, resident type II pneumocytes ($PCNA^-/SP\text{-}C^+$). **B** and **D**: The cells with positive staining were counted in 10 randomly selected microscopic fields of individual animals, and mean IHC scores were calculated. Original magnifications: ×630 (**A** and **B**). Black bars indicate number of resident type II pneumocytes ($SP\text{-}C^+$); white bars, number of newly proliferated type II pneumocytes ($PCNA^+/SP\text{-}C^+$). Proliferation index is defined as the number of proliferating type II pneumocytes ($PCNA^+/SP\text{-}C^+$) expressed as a percentage of total type II pneumocyte ($SP\text{-}C^+$) numbers. These observations were performed in three to four mice per time point. Data are shown as means ± SD. ND, not detected.

most animals dying within 9 days. In mice infected with H1N1 pdm 2009 virus, however, the extent of lung damage was mainly within the epithelial cells of the bronchus and bronchiole, with occasional alveolar injury. All of the H1N1 pdm 2009 virus-infected animals survived through 9 days after infection. After infection with H5N1 HPAIV, the viral titers in lung tissue increased through day 6 and decreased on day 9. (However, the 9-day values were derived only from the two of seven animals that survived to the ninth day after infection.) In mice infected with H1N1 pdm 2009 virus, the viral titers in lung tissue gradually decreased over time. Notably, many kinds of cells (eg, vascular endothelial cells, pneumocytes, some macrophages, and epithelial cells) were infected with H5N1 HPAIV. Thus, H5N1 HPAIV appears to exhibit a wide range of tissue tropism within cells of the lungs, replicating in many kinds of cells in the lungs and resulting in an exaggerated production of the virus.

H5N1 avian influenza[24] viruses are known to induce DAD in humans. In the lungs of fatal cases, H1N1 pdm 2009 virus induced DAD as a predominant pathological process of the lower respiratory tract, reflecting alveolar injury by both direct virus replication in pneumocytes and associated degeneration of the alveolar structures (probably by concurrent host immune processes).[25] Several reports have suggested that the presence in the lower respiratory tract of high-affinity receptors for the virus may be a key trigger in infection by swine-origin influenza virus.[26] In the human lower respiratory tract, H5N1 attaches predominantly to type II pneumocytes and alveolar macrophages, as well as to nonciliated cuboidal epithelial cells in terminal bronchioles; attachment becomes progressively rarer toward the trachea.[11] In the present study (in mouse), H1N1 pdm 2009 virus caused limited lung injuries, with little damage observed in the alveoli even 9 days after infection. In contrast, H5N1 HPAIV caused severe lung damage, which eventually extended from the bronchus to the alveoli. Although proliferation of type II pneumocytes was stimulated, the alveolar damage worsened and extended rapidly, finally developing into DAD. Extensive destruction resulted in severe alveolar collapse, accompanied by intra-alveolar hemorrhage by 9 days after infection. These virulent processes have been ascribed to H5N1 and to other types of influenza virus, including Spanish influenza virus H1N1 1918,[27] which showed highly pathogenic characters, and H3N2.[11,28,29] Although influenza virus NP protein was detected at low levels in the alveoli of mice infected with H1N1 pdm 2009 virus in the present study, alveolar damage was not remarkable in H&E-stained lung specimens. Proliferation of macrophages that may be newly proliferating macrophages or may be derived from infiltrating monocytes, as well as type II pneumocytes, was observed in these animals. H1N1 pdm 2009 virus–infected mice showed viral

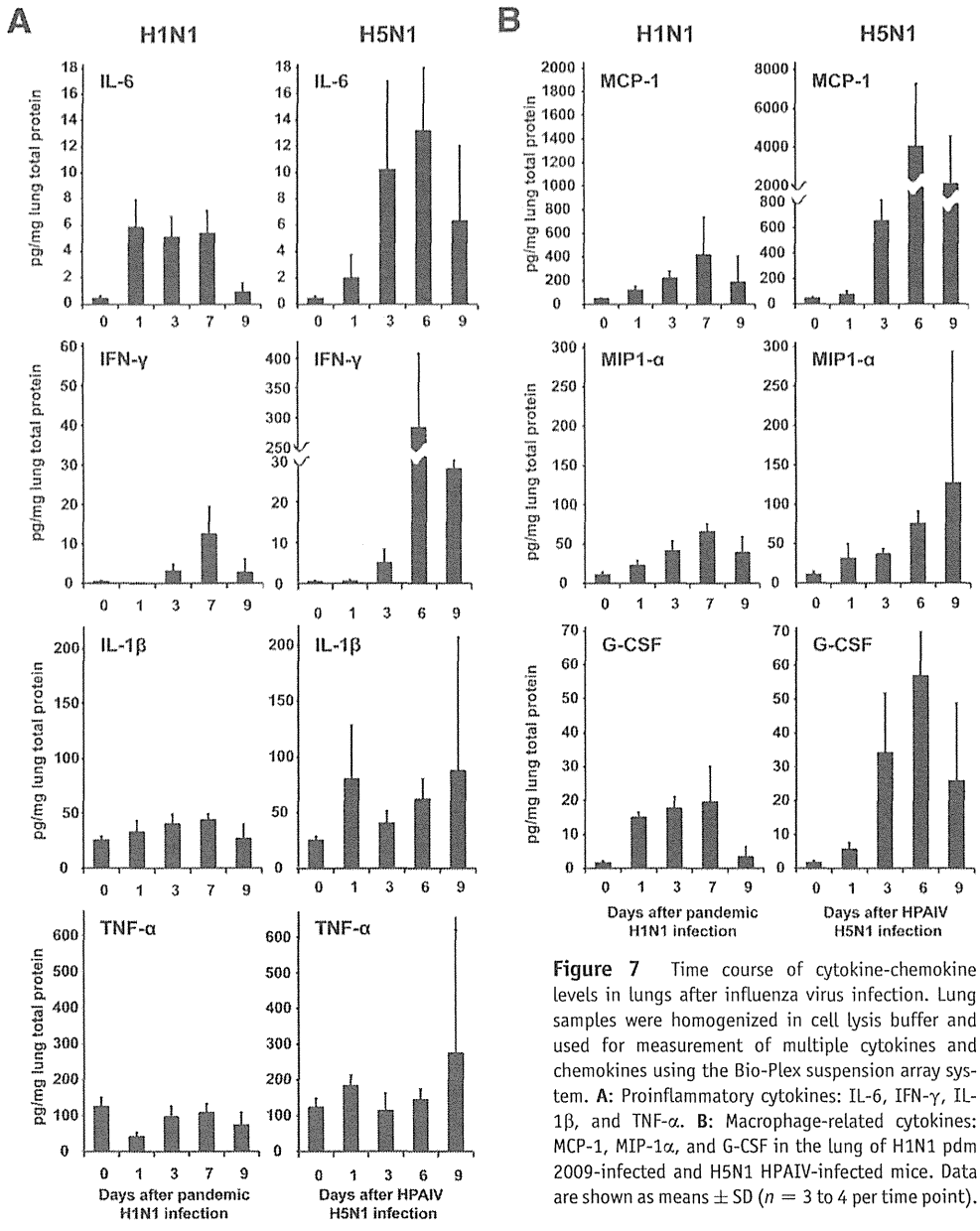

Figure 7 Time course of cytokine-chemokine levels in lungs after influenza virus infection. Lung samples were homogenized in cell lysis buffer and used for measurement of multiple cytokines and chemokines using the Bio-Plex suspension array system. **A:** Proinflammatory cytokines: IL-6, IFN-γ, IL-1β, and TNF-α. **B:** Macrophage-related cytokines: MCP-1, MIP-1α, and G-CSF in the lung of H1N1 pdm 2009-infected and H5N1 HPAIV-infected mice. Data are shown as means ± SD (n = 3 to 4 per time point).

clearance, suitable proliferation of these cells, and repair of alveolar damage.

The envelope of influenza virus contains two large surface-exposed glycoproteins: HA and neuraminidase. The former is responsible for attachment and penetration of virus into host cells, whereas the latter is responsible for budding of progeny virions from host cells. These molecules are important targets of the host immune response. The envelope encloses the NP, which includes both RNA-binding and polymerase domains. Viral antigen (HA) was detected using an mAb specific for H5N1-HA,[15] which was recently developed in our laboratory. We detected viral antigen in the epithelial cells of the lower respiratory tract, necrotic material, alveolar epithelium, macrophages, vascular endothelium, and perivascular lymphocytes. Staining for H5N1-HA or NP in paired serial sections of lung tissue revealed the presence of NP and H5N1-HA in overlapping regions of the lung, suggesting co-expression of these antigens. Because H5N1-HA expression constitutes the dominant proportion of protein production in influenza-infected cells, we speculate that histochemical staining for H5N1-HA will provide greater sensitivity than for NP.

H5N1 HPAIV likely infects type I pneumocytes, which cover 95% of the total alveolar surface; the resulting cytopathic destruction is expected to lead to alveolar damage,[30,31] which, in turn, would induce the proliferation of type II pneumocytes.[32] In the present study, we observed that type II pneumocytes infected with H5N1 HPAIV

exhibited extensive proliferation, with numbers peaking at 6 days after infection before decreasing at 9 days. The proliferation of type II pneumocytes is important for repairing alveolar damage, because type II pneumocytes differentiate into type I cells. We detected H5N1-HA antigen in type II pneumocytes, indicating that H5N1 HPAIV infected these cells. Because type II pneumocytes are metabolically active and are the most numerous cell type lining the alveoli after elimination of the type I pneumocytes, targeting of this cell type by virus is expected to lead to abundant virus production. Damage to type II pneumocytes may impair their functions, including re-epithelization of damaged alveoli, ion transport, and surfactant production; this may inhibit tissue repair. We speculate that acute proliferation of type II pneumocytes, as observed in the present study, prevents precise repair of the destroyed alveolar structures, with subsequent depletion of type II pneumocytes by viral cytopathic effects.

In the present study, many $PCNA^{+}$ macrophages persisted for 9 days after infection, in contrast to the temporary increase observed for type II pneumocytes. A massive infiltration of macrophages has been observed in the lungs of H5N1-infected humans and mice.[33–36] Targeting of macrophages by influenza virus may be important because of the role of macrophages in facilitating the host innate immune response to viral infection.[11] Other researchers also have suggested that influenza infection of macrophages stimulates production and release of proinflammatory cytokines and α/β interferon,[37] which may assist in limiting further viral replication and spread within the respiratory tract. Nonetheless, the lungs of the present study's H5N1 HPAIV-infected mice were severely damaged, with exaggerated replication of H5N1 HPAIV. By using IHC staining, we showed the presence of viral proteins in alveolar epithelial cells and macrophages in alveoli. In contrast, an *in situ* hybridization assay showed that viral RNA transcripts were detected largely in alveolar epithelial cells, but not in macrophages in alveoli. Although the discrepancy of the detection levels between viral protein and viral RNA in macrophages raises the possibility of the phagocytic processes of viral antigens in the macrophages, further study is required for clearing whether phagocytic ingestions of influenza virus antigens occur.

Double IHC staining for PCNA (proliferation of cells) and SP-C (type II pneumocytes) or Iba1 (macrophages) was used to assess the proliferation of macrophages or of type II pneumocytes, respectively, in the alveoli after murine infection with H5N1 HPAIV. We observed that macrophage proliferation increased progressively through the 9 days after infection. In contrast, the proliferation of type II pneumocytes peaked at 6 days after infection, before subsequently decreasing. This difference in the time course of reaction to viral infection between these two cell types may reflect distinct responses to infection by H5N1 HPAIV. The direct viral injury to type II pneumocytes may impair these cells' functions, including re-epithelialization after alveolar damage and surfactant production, thereby stalling tissue repair.[11] Excessive accumulation of macrophages in the lungs could contribute to tissue damage by causing vascular injury and destruction of the parenchymal cells.[38,39] Our cytokine-chemokine expression data supported these findings. In the present study, the response by macrophages appeared to be a major contributor to intense lung collapse.

In conclusion, intranasal infection of mice with H5N1 HPAIV resulted in intense viral replication in the lungs involving multiple cell types, with rapid progression of lung injuries leading to serious DAD. Proliferation of type II pneumocytes stalled the repair of alveolar damage. Hyperproliferation of macrophages that may be newly proliferating macrophages or may be derived from infiltrating monocytes appeared to impair defense against the viral attack, resulting in self-destruction. In mice infected with H1N1 pdm 2009 virus, adequate proliferation of the macrophages permitted successful defense against viral attack, and moderate proliferation of type II pneumocytes effectively repaired alveolar injuries. Thus, the lower respiratory tract was effectively excluded from the extent of lung injuries. We hypothesize that the virulence of H5N1 HPAIV results from the wide range of cell tropism of the virus, excessive virus replication in the lungs, and rapid development of injuries reaching to the alveoli.

Acknowledgments

We thank Drs. Satoshi Naganawa and Sumiko Gomi and Yoshimi Tobita for technical support and all members of our laboratory for their advice and assistance.

Supplemental Data

Supplemental material for this article can be found at *http://dx.doi.org/10.1016/j.ajpath.2013.10.004.*

References

1. Okamatsu M, Tanaka T, Yamamoto N, Sakoda Y, Sasaki T, Tsuda Y, Isoda N, Kokumai N, Takada A, Umemura T, Kida H: Antigenic, genetic, and pathogenic characterization of H5N1 highly pathogenic avian influenza viruses isolated from dead whooper swans (Cygnus cygnus) found in northern Japan in 2008. Virus Genes 2010, 41:351–357
2. Sakoda Y, Ito H, Uchida Y, Okamatsu M, Yamamoto N, Soda K, Nomura N, Kuribayashi S, Shichinohe S, Sunden Y, Umemura T, Usui T, Ozaki H, Yamaguchi T, Murase T, Ito T, Saito T, Takada A, Kida H: Reintroduction of H5N1 highly pathogenic avian influenza virus by migratory water birds, causing poultry outbreaks in the 2010-2011 winter season in Japan. J Gen Virol 2012, 93(Pt 3):541–550
3. Claas EC, Osterhaus AD, van Beek R, De Jong JC, Rimmelzwaan GF, Senne DA, Krauss S, Shortridge KF, Webster RG: Human influenza A H5N1 virus related to a highly pathogenic avian influenza virus. Lancet 1998, 351:472–477
4. To KF, Chan PK, Chan KF, Lee WK, Lam WY, Wong KF, Tang NL, Tsang DN, Sung RY, Buckley TA, Tam JS, Cheng AF: Pathology of fatal human infection associated with avian influenza A H5N1 virus. J Med Virol 2001, 63:242–246

5. Korteweg C, Gu J: Pathology, molecular biology, and pathogenesis of avian influenza A (H5N1) infection in humans. Am J Pathol 2008, 172: 1155–1170
6. Kuiken T, Taubenberger JK: Pathology of human influenza revisited. Vaccine 2008, 26(Suppl 4):D59–D66
7. de Jong MD: H5N1 transmission and disease: observations from the frontlines. Pediatr Infect Dis J 2008, 27:S54–S56
8. Garcia-Sastre A, Whitley RJ: Lessons learned from reconstructing the 1918 influenza pandemic. J Infect Dis 2006, 194(Suppl 2):S127–S132
9. van Riel D, Munster VJ, de Wit E, Rimmelzwaan GF, Fouchier RA, Osterhaus AD, Kuiken T: Human and avian influenza viruses target different cells in the lower respiratory tract of humans and other mammals. Am J Pathol 2007, 171:1215–1223
10. Chutinimitkul S, Herfst S, Steel J, Lowen AC, Ye J, van Riel D, Schrauwen EJ, Bestebroer TM, Koel B, Burke DF, Sutherland-Cash KH, Whittleston CS, Russell CA, Wales DJ, Smith DJ, Jonges M, Meijer A, Koopmans M, Rimmelzwaan GF, Kuiken T, Osterhaus AD, García-Sastre A, Perez DR, Fouchier RA: Virulence-associated substitution D222G in the hemagglutinin of 2009 pandemic influenza A(H1N1) virus affects receptor binding. J Virol 2010, 84:11802–11813
11. van Riel D, Munster VJ, de Wit E, Rimmelzwaan GF, Fouchier RA, Osterhaus AD, Kuiken T: H5N1 virus attachment to lower respiratory tract. Science 2006, 312:399
12. Reperant LA, Kuiken T, Grenfell BT, Osterhaus AD, Dobson AP: Linking influenza virus tissue tropism to population-level reproductive fitness. PLoS One 2012, 7:e43115
13. Zhang H: Tissue and host tropism of influenza viruses: importance of quantitative analysis. Sci China C Life Sci 2009, 52:1101–1110
14. Solecki D, Gromeier M, Harber J, Bernhardt G, Wimmer E: Poliovirus and its cellular receptor: a molecular genetic dissection of a virus/receptor affinity interaction. J Mol Recognit 1998, 11:2–9
15. Sakaguchi N, Kimura T, Matsushita S, Fujimura S, Shibata J, Araki M, Sakamoto T, Minoda C, Kuwahara K: Generation of high-affinity antibody against T cell-dependent antigen in the Ganp gene-transgenic mouse. J Immunol 2005, 174:4485–4494
16. Yewdell JW, Frank E, Gerhard W: Expression of influenza A virus internal antigens on the surface of infected P815 cells. J Immunol 1981, 126:1814–1819
17. Chan KH, Zhang AJ, To KK, Chan CC, Poon VK, Guo K, Ng F, Zhang QW, Leung VH, Cheung AN, Lau CC, Woo PC, Tse H, Wu W, Chen H, Zheng BJ, Yuen KY: Wild type and mutant 2009 pandemic influenza A (H1N1) viruses cause more severe disease and higher mortality in pregnant BALB/c mice. PLoS One 2010, 5:e13757
18. Trias EL, Hassantoufighi A, Prince GA, Eichelberger MC: Comparison of airway measurements during influenza-induced tachypnea in infant and adult cotton rats. BMC Pulm Med 2009, 9:28
19. Vincent AL, Thacker BJ, Halbur PG, Rothschild MF, Thacker EL: An investigation of susceptibility to porcine reproductive and respiratory syndrome virus between two genetically diverse commercial lines of pigs. J Anim Sci 2006, 84:49–57
20. Belser JA, Gustin KM, Maines TR, Blau DM, Zaki SR, Katz JM, Tumpey TM: Pathogenesis and transmission of triple-reassortant swine H1N1 influenza viruses isolated before the 2009 H1N1 pandemic. J Virol 2011, 85:1563–1572
21. Suzuki H, Aoshiba K, Yokohori N, Nagai A: Epidermal growth factor receptor tyrosine kinase inhibition augments a murine model of pulmonary fibrosis. Cancer Res 2003, 63:5054–5059
22. Imai Y, Kuba K, Neely GG, Yaghubian-Malhami R, Perkmann T, van Loo G, Ermolaeva M, Veldhuizen R, Leung YH, Wang H, Liu H, Sun Y, Pasparakis M, Kopf M, Mech C, Bavari S, Peiris JS, Slutsky AS, Akira S, Hultqvist M, Holmdahl R, Nicholls J, Jiang C, Binder CJ, Penninger JM: Identification of oxidative stress and toll-like receptor 4 signaling as a key pathway of acute lung injury. Cell 2008, 133:235–249
23. Miyanari Y, Atsuzawa K, Usuda N, Watashi K, Hishiki T, Zayas M, Bartenschlager R, Wakita T, Hijikata M, Shimotohno K: The lipid droplet is an important organelle for hepatitis C virus production. Nat Cell Biol 2007, 9:1089–1097
24. Maines TR, Lu XH, Erb SM, Edwards L, Guarner J, Greer PW, Nguyen DC, Szretter KJ, Chen LM, Thawatsupha P, Chittaganpitch M, Waicharoen S, Nguyen DT, Nguyen T, Nguyen HH, Kim JH, Hoang LT, Kang C, Phuong LS, Lim W, Zaki S, Donis RO, Cox NJ, Katz JM, Tumpey TM: Avian influenza (H5N1) viruses isolated from humans in Asia in 2004 exhibit increased virulence in mammals. J Virol 2005, 79:11788–11800
25. Basu A, Shelke V, Chadha M, Kadam D, Sangle S, Gangodkar S, Mishra A: Direct imaging of pH1N1 2009 influenza virus replication in alveolar pneumocytes in fatal cases by transmission electron microscopy. J Electron Microsc (Tokyo) 2011, 60:89–93
26. Yeh E, Luo RF, Dyner L, Hong DK, Banaei N, Baron EJ, Pinsky BA: Preferential lower respiratory tract infection in swine-origin 2009 A(H1N1) influenza. Clin Infect Dis 2010, 50:391–394
27. Tumpey TM, García-Sastre A, Taubenberger JK, Palese P, Swayne DE, Pantin-Jackwood MJ, Schultz-Cherry S, Solorzano A, Van Rooijen N, Katz JM, Basler CF: Pathogenicity of influenza viruses with genes from the 1918 pandemic virus: functional roles of alveolar macrophages and neutrophils in limiting virus replication and mortality in mice. J Virol 2005, 79:14933–14944
28. Seo SH, Webby R, Webster RG: No apoptotic deaths and different levels of inductions of inflammatory cytokines in alveolar macrophages infected with influenza viruses. Virology 2004, 329: 270–279
29. Shinya K, Ebina M, Yamada S, Ono M, Kasai N, Kawaoka Y: Avian flu: influenza virus receptors in the human airway. Nature 2006, 440: 435–436
30. Ng WF, To KF, Lam WW, Ng TK, Lee KC: The comparative pathology of severe acute respiratory syndrome and avian influenza A subtype H5N1—a review. Hum Pathol 2006, 37:381–390
31. Williams MC: Alveolar type I cells: molecular phenotype and development. Annu Rev Physiol 2003, 65:669–695
32. Wang J, Edeen K, Manzer R, Chang Y, Wang S, Chen X, Funk CJ, Cosgrove GP, Fang X, Mason RJ: Differentiated human alveolar epithelial cells and reversibility of their phenotype in vitro. Am J Respir Cell Mol Biol 2007, 36:661–668
33. Peiris JS, Yu WC, Leung CW, Cheung CY, Ng WF, Nicholls JM, Ng TK, Chan KH, Lai ST, Lim WL, Yuen KY, Guan Y: Re-emergence of fatal human influenza A subtype H5N1 disease. Lancet 2004, 363:617–619
34. Maines TR, Szretter KJ, Perrone L, Belser JA, Bright RA, Zeng H, Tumpey TM, Katz JM: Pathogenesis of emerging avian influenza viruses in mammals and the host innate immune response. Immunol Rev 2008, 225:68–84
35. Lee SM, Gardy JL, Cheung CY, Cheung TK, Hui KP, Ip NY, Guan Y, Hancock RE, Peiris JS: Systems-level comparison of host-responses elicited by avian H5N1 and seasonal H1N1 influenza viruses in primary human macrophages. PLoS One 2009, 4:e8072
36. Lee SM, Cheung CY, Nicholls JM, Hui KP, Leung CY, Uiprasertkul M, Tipoe GL, Lau YL, Poon LL, Ip NY, Guan Y, Peiris JS: Hyperinduction of cyclooxygenase-2-mediated proinflammatory cascade: a mechanism for the pathogenesis of avian influenza H5N1 infection. J Infect Dis 2008, 198:525–535
37. Peschke T, Bender A, Nain M, Gemsa D: Role of macrophage cytokines in influenza A virus infections. Immunobiology 1993, 189: 340–355
38. Azoulay E, Darmon M, Delclaux C, Fieux F, Bornstain C, Moreau D, Attalah H, Le Gall JR, Schlemmer B: Deterioration of previous acute lung injury during neutropenia recovery. Crit Care Med 2002, 30: 781–786
39. Mulligan MS, Watson SR, Fennie C, Ward PA: Protective effects of selectin chimeras in neutrophil-mediated lung injury. J Immunol 1993, 151:6410–6417

PLOS | ONE

RESEARCH ARTICLE

Diabetes Mellitus Accelerates Aβ Pathology in Brain Accompanied by Enhanced GAβ Generation in Nonhuman Primates

Sachi Okabayashi[1,2], Nobuhiro Shimozawa[1], Yasuhiro Yasutomi[1], Katsuhiko Yanagisawa[3], Nobuyuki Kimura[1,3]*

1 Tsukuba Primate Research Center, National Institute of Biomedical Innovation, 1–1 Hachimandai, Tsukuba-shi, Ibaraki, 305–0843, Japan, **2** The Corporation for Production and Research of Laboratory Primates, 1–1 Hachimandai, Tsukuba-shi, Ibaraki, 305–0843, Japan, **3** Section of Cell Biology and Pathology, Department of Alzheimer's Disease Research, Center for Development of Advanced Medicine for Dementia, National Center for Geriatrics and Gerontology (NCGG), Gengo 35, Moriika, Obu, Aichi, 474–8511, Japan

* kimura@ncgg.go.jp

Citation: Okabayashi S, Shimozawa N, Yasutomi Y, Yanagisawa K, Kimura N (2015) Diabetes Mellitus Accelerates Aβ Pathology in Brain Accompanied by Enhanced GAβ Generation in Nonhuman Primates. PLoS ONE 10(2): e0117362. doi:10.1371/journal.pone.0117362

Academic Editor: Yoshitaka Nagai, National Center of Neurology and Psychiatry, JAPAN

Received: July 20, 2014

Accepted: December 21, 2014

Published: February 12, 2015

Data Availability Statement: All relevant data are within the paper and its Supporting Information files.

Funding: This study was supported by The Research Funding for Longevity Sciences (25-20) from National Center for Geriatrics and Gerontology (NCGG), Japan. The funders had no role in study design, data collection and analysis, decision to publish, or preparation of the manuscript.

Competing Interests: The authors have declared that no competing interests exist.

Abstract

Growing evidence suggests that diabetes mellitus (DM) is one of the strongest risk factors for developing Alzheimer's disease (AD). However, it remains unclear why DM accelerates AD pathology. In cynomolgus monkeys older than 25 years, senile plaques (SPs) are spontaneously and consistently observed in their brains, and neurofibrillary tangles are present at 32 years of age and older. In laboratory-housed monkeys, obesity is occasionally observed and frequently leads to development of type 2 DM. In the present study, we performed histopathological and biochemical analyses of brain tissue in cynomolgus monkeys with type 2 DM to clarify the relationship between DM and AD pathology. Here, we provide the evidence that DM accelerates Aβ pathology *in vivo* in nonhuman primates who had not undergone any genetic manipulation. In DM-affected monkey brains, SPs were observed in frontal and temporal lobe cortices, even in monkeys younger than 20 years. Biochemical analyses of brain revealed that the amount of GM1-ganglioside-bound Aβ (GAβ)—the endogenous seed for Aβ fibril formation in the brain—was clearly elevated in DM-affected monkeys. Furthermore, the level of Rab GTPases was also significantly increased in the brains of adult monkeys with DM, almost to the same levels as in aged monkeys. Intraneuronal accumulation of enlarged endosomes was also observed in DM-affected monkeys, suggesting that exacerbated endocytic disturbance may underlie the acceleration of Aβ pathology due to DM.

Introduction

Alzheimer's disease (AD) is a progressive neurological disorder that is histopathologically characterized by the formation of senile plaques (SPs) and neurofibrillary tangles (NFTs) [1, 2]. It is widely accepted that β-amyloid protein (Aβ), the major component of SPs, is a key molecule

underlying AD pathogenesis [3, 4]. Several epidemiological/clinical studies have shown that diabetic mellitus (DM) patients are significantly more likely to develop cognitive dysfunction and exhibit increased susceptibility to AD [5–9], in consistent with the original Rotterdam study [10]. Recent findings also showed that there are several pathogenic connections between AD and DM patient brains, such as brain inflammation, mitochondrial dysfunction, and defective neuronal insulin signaling [11]. Insulin resistance causes alteration in GSK3β kinase signaling pathway as observed in AD brains, and it is also associated with an AD-like pattern of reduced cerebral glucose metabolic rate in brain [12, 13]. Moreover, accumulating evidences showed that the experimental induction of DM enhanced AD pathology even in rodents [14–25]. However, it remains unclear how DM physiologically accelerates AD pathology in the brain.

With advancing age, both SPs and NFTs occur spontaneously in brains of cynomolgus monkeys [26, 27]. In addition, the amino acid sequence of Aβ of cynomolgus monkeys is completely consistent with that of humans [28]. These advantages make this species a useful model to study age-dependent AD pathophysiology. As with humans, obesity occasionally occurs in adult, middle-aged monkeys, and it can result in the development of type 2 DM [29, 30]. Similar to the case of humans, these monkeys have a period of insulin resistance and hyperinsulinemia before developing overt DM, which is then accompanied by deficiency in pancreatic insulin production [29–31]. The pathological changes that occur in the pancreatic islets of aged monkeys are also similar to those seen in human diabetics, including the deposition of islet amyloid polypeptide (IAPP) [29–31]. In addition, gestational diabetes has been also reported in female cynomolgus monkeys [29–31]. Thus, cynomolgus monkeys are a useful species to investigate not only age-dependent AD lesions but also the relationship between DM and AD pathology.

Here, we report that DM enhances the generation of GM1-ganglioside-bound Aβ (GAβ) to accelerate SP deposition in cynomolgus monkey brains. GAβ was previously identified as the endogenous seed for Aβ fibril formation in the brain, and its generation is enhanced by endocytic disturbance, which is considered to be involved in early-stage AD pathology [32–34]. In DM-affected adult monkeys, the level of Rab GTPases in the brain was obviously increased as compared to normal adult monkeys, and intraneuronal endosomes were apparently enlarged. These findings suggest that DM exacerbates age-dependent endocytic disturbance, which then may lead to accelerate Aβ pathology via enhanced GAβ generation.

Materials and Methods

Animals

Forty-one cynomolgus monkey (*Macaca fascicularis*) brains were used in this study. Of these, six brains were from young monkeys (age: 6 and 7 years); six were from normal adult monkeys (age: 17, 18, 19, and 20 years); nine were from DM-affected adult monkeys (age: 17, 18, 19, and 20 years); ten were from normal aged monkeys (age: 24, 25, 26, and 28 years); and ten were from DM-affected aged monkeys (age: 24, 25, 26, and 28 years). The frontal and temporal lobes were used for immunohistochemical studies. The cerebral cortices of 12 monkeys were used for dot blot analyses. Of these 12, 3 were from young monkeys (age: 6 years [N = 2] and 7 years [N = 1]); 3 were from normal adult monkeys (age: 18 years, 19 years, and 20 years [N = 1 each]); 3 were from DM-affected adult monkeys (age: 18 years, 19 years, and 20 years [N = 1 each]); and 3 were from normal aged monkeys (age: 26 years [N = 2] and 28 years [N = 1]). The cerebral cortices of 12 female monkeys were used for Western blot analyses. Of these 12, 3 were from young monkeys (age: 7 years [N = 3]); 3 were from normal adult monkeys (age: 18 years, 19 years, and 20 years [N = 1 each]); 3 were from DM-affected adult monkeys (age: 18 years, 19 years, and 20 years [N = 1 each]); and 3 were from normal aged monkeys (age: 25 years and 26 years [N = 2]). The cerebral cortices of 14 female monkeys were used for

Aβ ELISA. Of these 12, 4 were from young monkeys (age: 7 years [N = 4]); 3 were from normal adult monkeys (age: 18 years, 19 years, and 20 years [N = 1 each]); 3 were from DM-affected adult monkeys (age: 18 years, 19 years, and 20 years [N = 1 each]); and 4 were from normal aged monkeys (age: 24 years [N = 3], and 25 years [N = 1]). All brains were obtained from the Tsukuba Primate Research Center (TPRC), National Institute of Biomedical Innovation (NIBIO), Japan. Monkeys in the TPRC are reared in individual cages (0.5 m wide × 0.8 m high × 0.9 m deep; stain-less steel mesh). The breeding rooms are rectangular, and the individual cages are installed on the long sides of the room. Each room contains at least 90 cages. Therefore, monkeys can always make visual, auditory and olfactory contact with their roommates. Ambient temperature in the rooms is kept about 25°C, and humidity is set at 50% to 60%. The air is replaced 12 times hourly. Monkeys are provided with 100 g of apples in the morning, and 70 g of commercial food (Type AS; Oriental Yeast Co., Ltd., Tokyo, Japan) is given to them twice in the afternoon. Water is available ad libitum. Every morning their health status (e.g., viability, appetite, fur-coat appearance) was monitored by experienced animal technicians. When any abnormality is found, a veterinarian examines the monkey promptly and applies the appropriate treatment. Moreover, the monkeys are medically examined under anesthesia (ketamine hydrochloride) at least once every 2 y. The medical examination consists of body weight measurement, tuberculin test, blood sample, stool test, examination of the fundus, and a medicated bath. The maintenance of animals was conducted according to the rules for animal care of the TPRC at NIBIO for the care, use, and biohazard countermeasures of laboratory animals [35]. This study was carried out in strict accordance with the recommendations in the Animal Care and Use Committee of the NIBIO, Japan. The protocol was approved by the Committee on the Ethics of Animal Experiments of the NIBIO (DS17-001R1). When the monkey presents clinical symptoms by injury or illness and it could not expect recovery from pain or morbidity, it is judged as poor prognosis. In the present study, the animals used in this study died of natural causes were euthanized when they reached endpoints determined as poor prognosis. All DM-affected monkeys were also sacrificed because of poor prognosis. For euthanasia, the monkeys were deeply anesthetized with a lethal dose of pentobarbital, and all efforts were made to minimize suffering.

Antibodies

In this study, we used the following antibodies: mouse monoclonal anti-dynein heavy chain (DHC) (Sigma, Saint Louis, MO); mouse monoclonal anti-dynein intermediate chain (DIC) (Millipore, Temecula, CA); mouse monoclonal anti- GAβ antibody (4396C) (22); mouse monoclonal kinesin light chain (KLC) (Santa Cruz Biotechnology, Santa Cruz, CA); mouse monoclonal anti-neprilysin (NEP; DAKO, Glostrup, Denmark); mouse monoclonal anti-phosphorylated tau antibody (AT8; Innogenetics, Gent, Belgium); mouse monoclonal anti-Rab5 antibody (Rab5m; Santa Cruz Biotechnology); rabbit polyclonal anti-Aβ antibody (IBL); rabbit polyclonal anti-full-length β-amyloid precursor protein (APP) antibody (IBL); rabbit polyclonal anti-Cathepsin D (CatD; Cell Signaling Technology, Danvers, MA); rabbit polyclonal anti-kinesin heavy chain (KHC) (Sigma); rabbit polyclonal anti-LC3 (Novus Biologicals, Littleton, CO); rabbit polyclonal anti-Rab5 antibody (Santa Cruz Biotechnology); rabbit polyclonal anti-Rab7 antibody (Sigma); rabbit polyclonal anti-Rab11 antibody (Santa Cruz Biotechnology); and rabbit polyclonal anti-synaptophysin (DAKO).

Histopathological analyses for DM-associated pathology

Most of the tissues were fixed in 10% neutral buffered formalin, processed routinely and stained with hematoxylin and eosin (HE) for histopathological analyses. The pancreases were also stained with direct fast scarlet (DFS; Muto) for identification of islet amyloid.

Immunohistochemistry

Brain samples were immersion-fixed in 10% neutral buffered formalin, embedded in paraffin, and cut into 4 μm-thick sections. For immunohistochemical analyses with anti-GAβ antibody, brain samples were fixed in 4% paraformaldehyde. Sections were deparaffinized by pretreatment with 0.5% periodic acid, and then incubated overnight at 4°C free floating in the following primary antibody solutions: (1) Aβ (1:100); (2) APP (1:100); (3) Rab5 (1:100); (4) GAβ (1:20); or (5) AT8 (1:100). Following brief washes with buffer, the sections were sequentially incubated with biotinylated goat anti-mouse IgG (1:200) or goat anti-rabbit IgG (1:200), followed by streptavidin-biotin-horseradish peroxidase complex (DAKO). Immunoreactive elements were visualized by treating the sections with 3–3' diaminobenzidine tetroxide (Dojin Kagaku). The sections were then counterstained with hematoxylin. The immunoreactivity of Aβ, GAβ, APP or Rab5 in a given cortical area was quantified with computer software Image J 1.49i (National Institue of Health). For quantification analyses, the sections were not counterstained with hematoxylin.

Biochemical analyses of monkey brains

Frozen monkey brain tissue (wet weight 0.2 g) was homogenized in a glass homogenizer with 4 ml of homogenate buffer solution (0.32 M sucrose, 10 mM Tris-HCl [pH 7.6], 0.25 mM PMSF, and 1 mM EDTA, and Complete Mini proteinase inhibitor cocktail), and then centrifuged at 100,000xg for 20 min to obtain the supernatant fraction. The proteins in the fraction were subjected to dot blot analyses. Brain homogenates were also centrifuged at 1,000×g for 10 min to remove the nuclear fraction, and then the supernatant was centrifuged at 105,000×g for 60 min to obtain the microsomal fraction. The proteins in the microsomal fraction were subjected to Western blot analyses. For Aβ ELISA, brain homogenates were incubated with Triton-X100 at a final concentration of 1% for 15 min at 37°C, and spun at 100,000 × g for 20 min at 20°C. The pellet was homogenized in homogenate buffer containing 1% sarkosyl, incubated for 15 min at 37°C, and spun at 100,000 × g for 20 min at 20°C. The sarkosyl-insoluble pellet was sonicated in 70% folic acid, cleared by centrifugation at 100,000 × g for 20 min at 20°C. The supernatant was evaporated, and then resuspended in dimethyl sulfoxiside (Sigma).

Dot blot analyses

Dot blot analyses were performed to assess age- and DM-related changes in GAβ formation. Brain samples were adjusted to 1 mg, 2.5 mg, and 5 mg, and then applied onto nitrocellulose membranes and dried. The membranes were blocked with 5% nonfat dried milk in 20 mM PBS (pH 7.0) and 0.1% Tween-20 for 1 h at room temperature, and then incubated in the anti-GAβ antibody solution overnight at 4°C. They were then incubated with horseradish peroxidase-conjugated goat anti-mouse IgG (1:10000; Cell Signaling Technology) for 1 h at room temperature. Immunoreactive elements were visualized using enhanced chemiluminescence (Luminata Forte Western HRP Substrate, Millipore).

Western blot analyses

Western blot analyses were performed to assess age- and DM-related changes in APP, Rab5, Rab7, Rab11, DHC, DIC, KHC, KLC, NEP, Cathepsin D heavy chain (CatD HC), and LC3 expression. Each microsome fraction prepared as described above was adjusted to 5 mg, and then analyzed using SDS-polyacrylamide gel electrophoresis using 14% (for LC3) or 12.5% (other proteins) acrylamide gels. Separated proteins were blotted onto polyvinylidense fluoride membranes (Immobilon P; Millipore). The membranes were blocked with 5% nonfat dried milk in

20 mM PBS (pH 7.0) and 0.1% Tween-20 for 1 h at room temperature, and then incubated overnight at 4°C in the following primary antibody solutions: (1) synaptophysin (1:20000); (2) APP (1:2000); (3) Rab5m (1:2000); (4) Rab7 (1:10000); (5) Rab11 (1:2000); (6) DHC (1:1000); (7) DIC (1:20,000); (8) KHC (1:5,000); (9) KLC (1:1000); (10) NEP (1:4,000); (11) CatD (1:2,000); or (12) LC3 (1:2,000). They were then incubated with either horseradish peroxidase-conjugated goat anti-mouse IgG or goat anti-rabbit IgG (1:10,000; Cell Signaling Technology) for 1 h at room temperature. Immunoreactive elements were visualized using enhanced chemiluminescence. To confirm reproducibility, immunoreactive bands obtained from the Western blots were quantified using commercially available software (Quantity One; PDI, Inc.).

Aβ ELISA

Total Aβ levels in young monkey, normal adult monkey, DM-affected monkey, and normal aged monkey brains were determined using a sandwich ELISA. The kit for Aβ (1-X) was obtained from IBL (Gunma, Japan). The ELISA assay was carried out according to the instruction manual. All samples were measured in duplicate.

Data analyses

Data obtained from quantitative analyses of immunohistochemistry and biochemical analyses are shown as means ± SD. For statistical analyses, one-way ANOVAs were performed, followed by the Fisher's post hoc test.

Results

Clinical background and DM-associated pathology in cynomolgus monkeys

Tsukuba Primate Research Center (TPRC) maintains a large breeding and rearing colony of cynomolgus monkeys for high-quality production of nonhuman primate models and biomedical investigations. In the TPRC colony, some adult monkeys are spontaneously affected with type 2 DM for various reasons, such as pregnancy history and environmental factors. The clinical background of all monkeys used for this study is shown in (S1 Table). TPRC has accumulated clinical data for more than 40 years. Based on these data, the normal blood glucose level for female monkeys is in the range of 24 to 74 mg/dL, and for male monkeys the range is 24 to 76 mg/dL. Normal blood triglyceride levels are in the range of 8 to 85 mg/dL for females, and 6 to 52 mg/dL for males. The blood glucose and triglyceride levels of normal adult monkeys used in the present study were all in the normal range, and their body weights were in the range of historical TPRC data for normal monkeys (S1 Table). All DM-affected monkeys, on the other hand, exhibited hyperlipidemia and hyperglycemia (S1 Table). These DM-affected monkeys were severely obese; however, their body weight at acquisition of their brains for this study had decreased to about less than half the maximum body weights they attained during their lifetime (S1 Table).

Histopathologically, islet amyloid was found in the pancreases of all DM-affected adult monkeys (Fig. 1A). In eight DM cases, most hyalinized islets were replaced with severe amyloid deposits, with the remaining islet cells being severely degenerated or decreased in apparent number (Fig. 1A-C). The hyalinized islets with severe amyloid deposits stained positive for direct fast scarlet (DFS) (Fig. 1D). Furthermore, two DM cases had fatty degeneration of the liver, and one DM case had mild atheromatosis. Thus, histopathological analyses demonstrated that these adult monkeys clearly had DM. On the other hand, we did not observe apparent vascular lesions in all DM monkey brains.

DM accelerates Aβ pathology in cynomolgus monkey brain

Next, we conducted immunohistochemical analyses to assess whether DM affects AD pathology in these cynomolgus monkey brains. As previously reported [26, 36], we observed SP depositions in the brains of aged monkeys (Fig. 2A), but not in those of normal adult monkeys younger than 20 years of age (Fig. 2B-D). Strikingly, we apparently observed diffuse Aβ-immunopositive SPs in brains of six DM-affected adult monkeys younger than 20 years old, even though they were very small quantities as compared to aged monkey brains (Fig. 2E-I). In aged cynomolgus monkey brains, cerebral amyloid angiopathy (CAA) lesions are also observed, and NFTs are observed over 32-year-old monkey brains [26, 27]. Although abnormally phosphorylated tau accumulation was not observed, we found much severe CAA in the brains of aged monkeys with DM (Fig. 3).

DM enhances GAβ generation in adult monkey brains

To assess whether DM affects Aβ level in monkey brains, we examined Aβ ELISA analyses. In aged monkey brains, Aβ level was significantly increased, suggesting that the increase of Aβ level correlates with age-dependent SP depositions (Fig. 4A). However, surprisingly, Aβ level was just slightly increased in DM-affected adult monkey brains as compared to normal adult monkey brains (Fig. 4A). We previously identified a unique Aβ species, called GAβ, characterized by its binding to GM1 ganglioside; GAβ was demonstrated in brain tissue along with early pathological changes characteristic of AD [32]. Accumulating evidence suggests that GAβ accelerates Aβ fibril formation by acting as a seed molecule [37–40]. We have also confirmed age-dependent GAβ generation in cynomolgus monkey brains [32, 41].

To test our hypothesis that DM enhances GAβ generation in the brain, we performed additional immunohistochemical analyses using an anti-GAβ-specific antibody. In the brains of normal adult monkeys, we observed little, if any, immunoreactivity with anti-GAβ antibody (Fig. 4B). In contrast, in the brains of DM-affected adult monkeys, we frequently observed neurons clearly immunopositive for anti-GAβ antibody (Fig. 4B). Quantitative analyses also confirmed that the immunoreactivity of GAβ was significantly increased in DM-affected adult monkey brains (Fig. 4C).

For biochemical analyses, we carried out dot blot analyses on monkey brain samples. Because of its conformational features, GAβ is not recognized by western blot analyses. Our dot blot analyses showed that GAβ generation increased in an age-dependent manner in cynomolgus monkey brains (Fig. 4D). GAβ immunoreactivity was much stronger in aged monkey brains, indicating that the amount of GAβ generated generally parallels age-dependent SP deposition as well as Aβ level. In normal adult monkey brains, the amount of GAβ generation was not much different from that in young monkey brains (Fig. 4D). It is noteworthy that GAβ generation was significantly increased in DM-affected adult monkey brains (Fig. 4E).

DM exacerbates endocytic disturbance with significant increase of Rab GTPases

In the brains of early-stage AD patients, neuronal endocytic pathology, such as intracellular accumulation of abnormally enlarged endosomes, is frequently observed [42–44]. We previously demonstrated that aging causes endocytic pathology along with a significant increase in Rab GTPases, resulting in the intracellular accumulation of APP [45]. This endocytic disturbance was observed in brains from cynomolgus monkeys almost 10 years before SP deposition begins [46]. We also reported that GAβ accumulates in enlarged endosomes of neurons in aged cynomolgus monkey brains [33]. Moreover, endocytic disturbance induces GAβ generation [34].

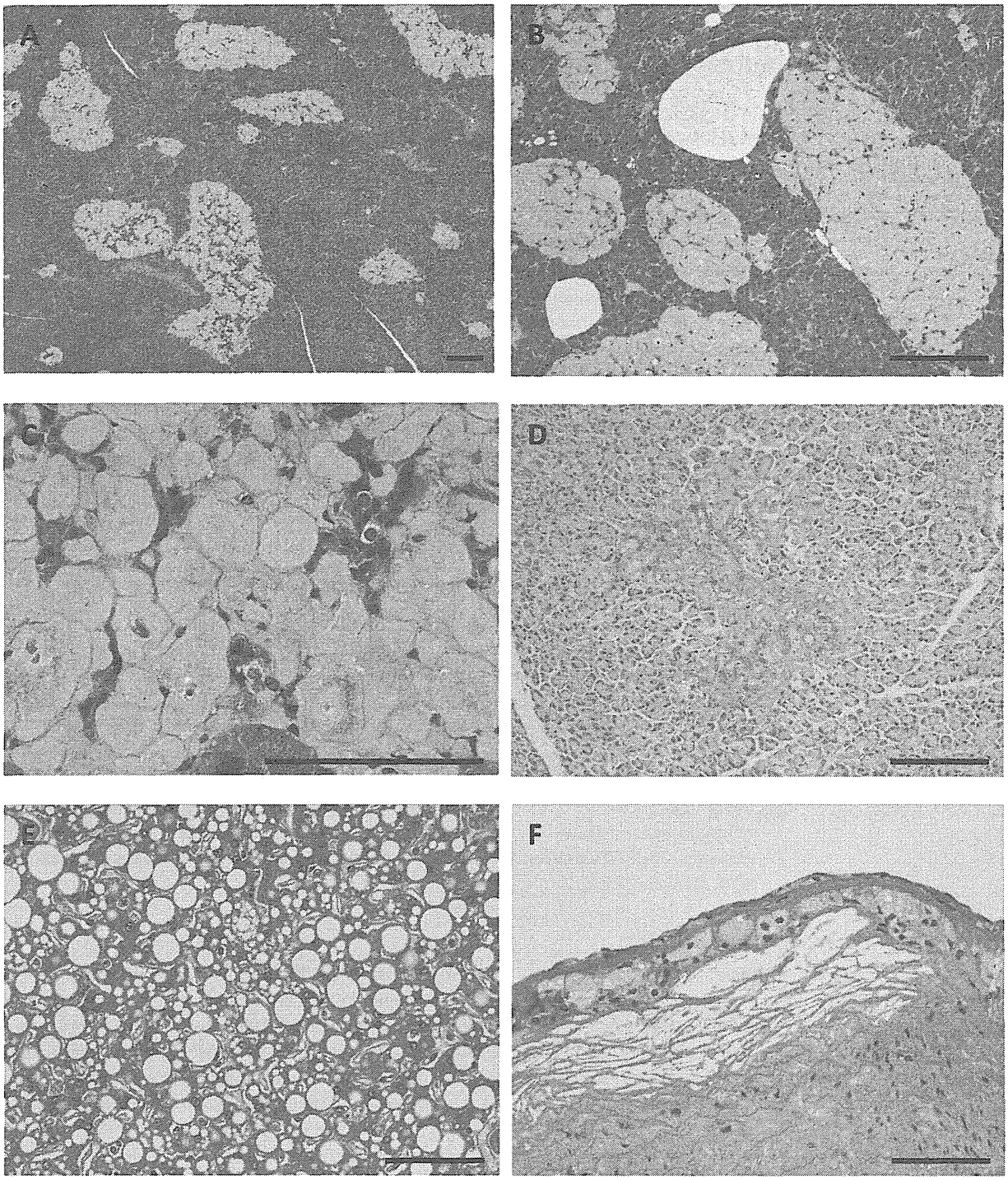

Fig 1. Histopathology of adult monkeys with type 2 diabetes mellitus. (A) Hematoxylin-eosin (HE)-stained section of the pancreas from a 17-year-old cynomolgus monkey with type 2 diabetes mellitus (DM) (S1 Table, Number 1). Most of the islets were replaced by abundant amyloid deposits. (B) HE-stained section of the pancreas from an 18-year-old cynomolgus monkey with DM (S1 Table, Number 3). Most of the islets were replaced with severe amyloid deposits. (C) HE-stained section of the pancreas from a 19-year-old cynomolgus monkey with DM (S1 Table, Number 7) showing hyalinized islets. Very few

islet cells remain. (D) Direct fast scarlet-stained section of pancreas from an 18-year-old cynomolgus monkey with DM (S1 Table, Number 5). Hyalinized islets with severe amyloid deposition were positive for direct fast scarlet staining. (E) HE-stained section of the liver from an 18-year-old cynomolgus monkey with DM (S1 Table, Number 3). Marked fatty degeneration was observed in the liver. (F) HE-stained section of the aorta from an 18-year-old cynomolgus monkey with DM (S1 Table, Number 5). Mild atheromatosis with foam cells and sterol clefts was observed in the aorta. Scale bars for a-f, 100 μm.

doi:10.1371/journal.pone.0117362.g001

Taken together, these findings suggest that endocytic disturbance is involved in age-dependent Aβ pathology. Thus, to assess whether DM enhances endocytic disturbance, we investigated endocytic pathology in monkey brains.

In the brains of normal adult monkeys, APP and Rab5-positive early endosomes were observed as small granules in neurons (Fig. 5A, B). By contrast, in the brains of DM-affected adult monkeys, the immunoreactivity of APP and Rab5 was significantly stronger and the immunopositive granules were larger (Fig. 5C, D). Quantitative analyses confirmed that both APP- and Rab5-immunopositive granules were significantly increased in DM-affected adult monkey brains as compared to normal adult monkey brains (Fig. 5E). Western blot analyses showed that Rab5, Rab7 (late endosome-associated GTPase), and Rab11 (recycling endosome-associated GTPase) were increased in aged monkey brains, corroborating that age-dependent endocytic disturbance does occur in monkey brains, as previously reported (Fig. 5F, G) [45]. The amount of APP was also significantly increased in aged monkey brains as previously reported (Fig. 5F, G) [45, 47]. In the brains of DM-affected adult monkeys, Rab GTPases and APP levels were apparently increased compared to the brains of normal adult monkeys, being almost same as in aged monkey brains (Fig. 5F, G).

DM affects cathepsin D level and autophagosome clearance

Endosome trafficking is mediated by axonal transport motor proteins [48], and a recent study showed that the experimental induction of DM alters axonal motor protein levels in rodent model [49]. In the present study, we did not find apparent differences in axonal motor protein levels between normal and DM-affected adult monkey brains (Fig. 6). Endocytic disturbance is also induced by the breakdown in lysosomal degradation [50]. In DM-affected adult monkey brains, the level of cathepsin D (CatD) heavy chain increased (Fig. 6). On the other hand, we observed the significant increase in autophagosome marker LC3-II level without any alterations in LC3-I level (Fig. 6). A recent study also showed that DM-associated down-regulation of insulin signals reduces the level of Aβ degrading enzymes such as neprilysin (NEP) [51]. However, we did not find a clear reduction tendency in NEP levels in the brains of DM-affected adult monkeys (Fig. 6).

Discussion

Here, we present the evidence that DM accelerates Aβ pathology in the brain parenchyma of nonhuman primates, which have not undergone any genetic manipulation. We demonstrated that DM does so by enhancing the generation of GAβ, the endogenous seed for Aβ fibril formation in the brain. The brains of DM-affected adult monkeys contained robust endocytic pathology, such as a significant increase in Rab GTPases and intraneuronal accumulation of enlarged endosomes. Endocytic disturbance is a cellular pathological characteristic of neurons of AD patients and enhances GAβ generation [33, 34]. Thus, our present findings suggest that DM exacerbates age-dependent endocytic disturbance, which in turn enhance GAβ generation resulting in accelerated Aβ pathology.

Recent epidemiological/clinical studies suggest that DM is a major risk factor for developing AD [5–9]. However, the underlying mechanisms for this association remain unclear. Thus, in the present study, we performed histopathological and biochemical analyses using brains from

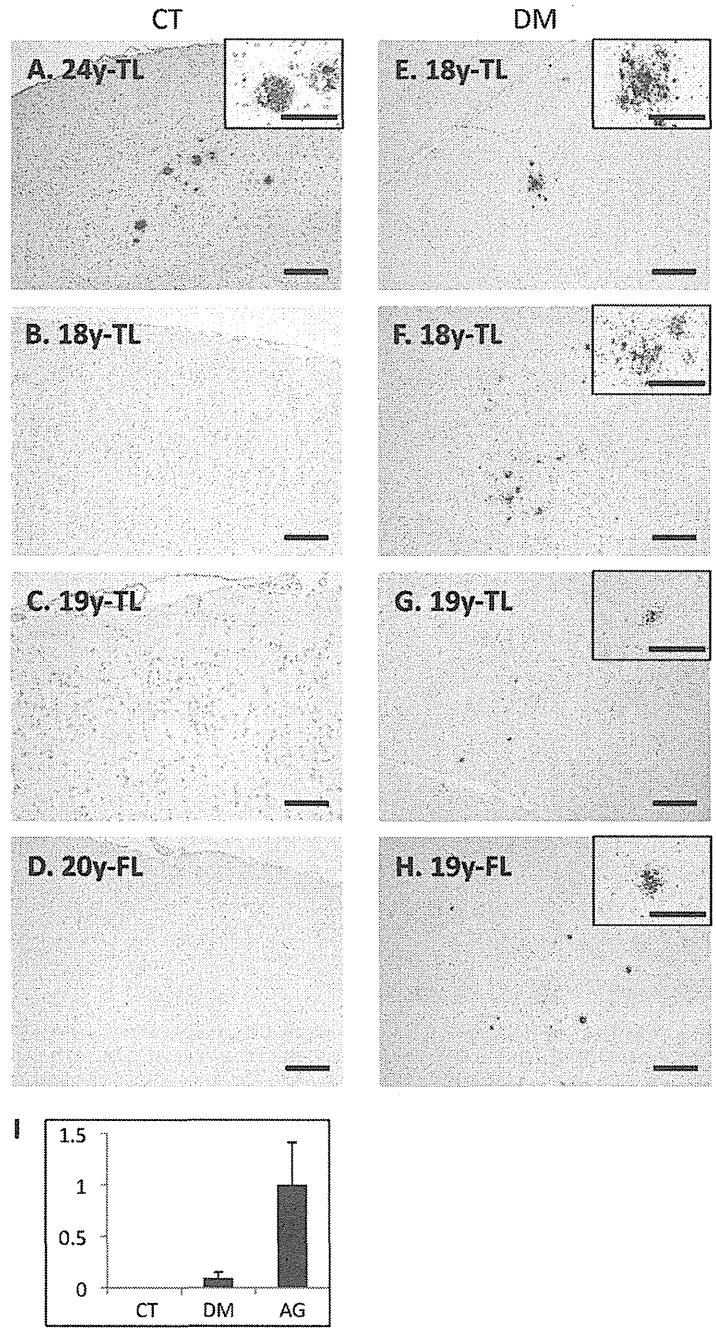

Fig 2. Senile plaques in the brains of adult monkeys with DM. Images of temporal lobe (TL) and frontal lobe (FL) sections from normal cynomolgus monkeys (A-D) and cynomolgus monkeys with DM (E-H). Sections were immunostained with anti-Aβ antibody and counterstained with hematoxylin. In aged monkey brains, we observed SPs immunostained with anti-Aβ antibody, as previously reported (A). In contrast, we did not observe Ab-immunopositive structures in the normal adult monkey brains (B-D). However, we did observe small but obvious Aβ-immunopositive senile plaques (SPs) in the frontal and temporal cortices of DM-affected adult monkeys (E-H). Scale bars, 100 μm. (I) Quantitative image analysis of Ab-immunopositive area in the sections obtained from female normal adult monkey, DM-affected adult monkey, and normal aged monkey brains. Data obtained from normal aged monkey brains were set as standards. Y-axes show the mean values of the quantified data. CT, normal cynomolgus monkeys. DM, DM-affected monkeys.

doi:10.1371/journal.pone.0117362.g002

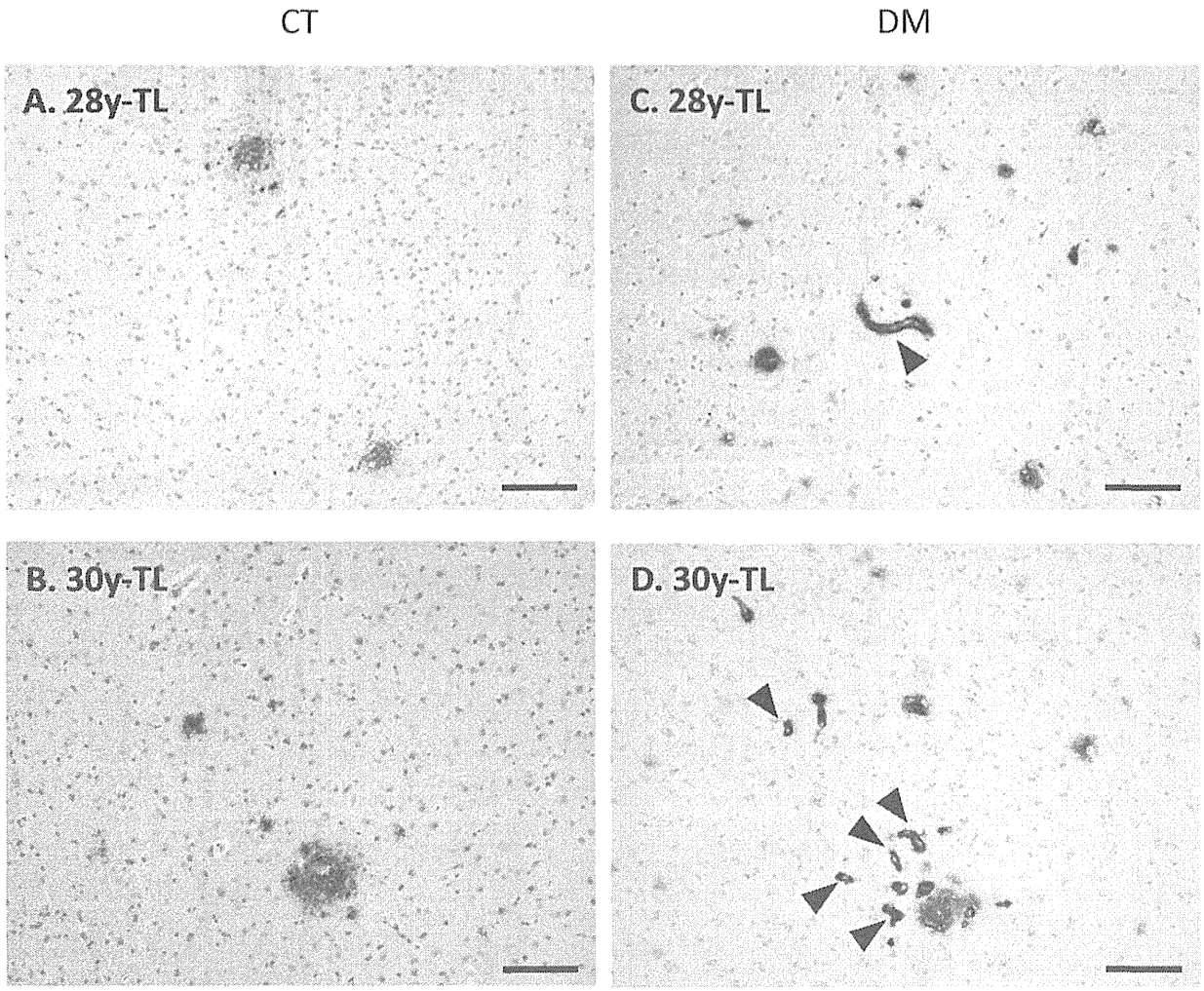

Fig 3. Cerebral amyloid angiopathy in the brains of aged monkeys with DM. Images of temporal lobe (TL) sections from normal cynomolgus monkeys (A, B) and cynomolgus monkeys with DM (C, D). Sections were immunostained with anti-Aβ antibody and counterstained with hematoxylin. In the brains of DM-affected aged monkeys, we observed very severe CAA lesions (arrowheads) as compared to normal aged monkeys. CT, normal aged monkeys. DM, DM-affected aged monkeys. Scale bars, 100 μm.

doi:10.1371/journal.pone.0117362.g003

DM-affected cynomolgus monkeys in order to assess the relationship between DM and AD pathology. As previously reported, SPs spontaneously form in the brains of aged monkeys over the age of 25 years, but never in the brains of normal young monkeys and adult monkey younger than 20 years (Fig. 2A-D) [26]. Strikingly, our immunohistochemical analyses revealed SP depositions in the brains of DM-affected adult monkeys as young as 18 years (Fig. 2E-H). To our knowledge, this is the first study to show that DM enhances Aβ pathology even in nonhuman primate brains without genetic manipulation. We also observed much severe CAA lesions in the brains of DM-affected aged monkeys than in those of normal aged monkeys (Fig. 3). These findings are consistent with the previous studies showing that DM-related conditions induce amyloidogenesis and Aβ pathology in rodent models [14–25]. Although additional

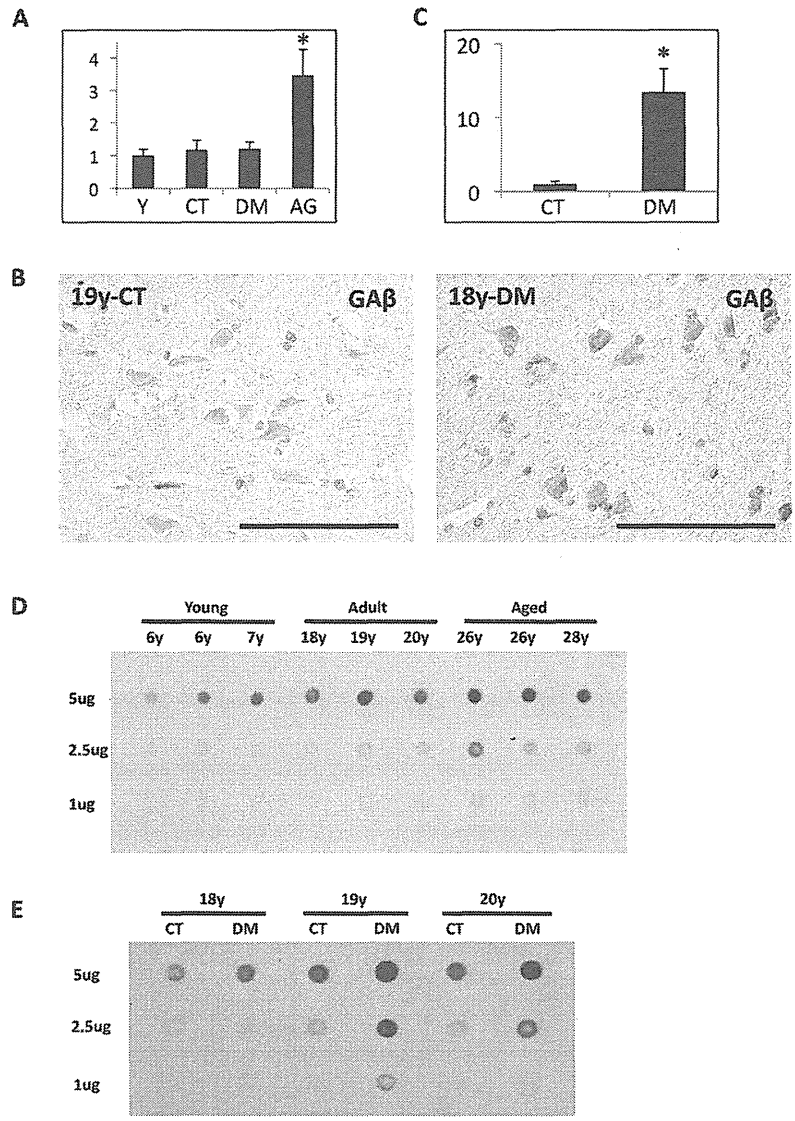

Fig 4. The analyses of Aβ and GAβ in the brains of normal and DM-affected monkeys. (A) Aβ level in young monkey, normal adult monkey, DM-affected monkey, and normal aged monkey brains were assessed with sandwich ELISA. Aβ level was significantly increased in normal aged monkey brains. In DM-affected monkey brains, Aβ level seemed unchanged. Data obtained from young monkey brains were set as standards. Y-axes show the mean values of the quantified data. Values are means ± SD. *P < 0.02. (B) Image of temporal lobe sections from a 19-year-old normal adult monkey and an 18-year-old cynomolgus monkey with DM. Sections were immunostained with the anti-GAβ-specific antibody 4396C and counterstained with hematoxylin. In the brain of the normal adult monkey, we observed little, if any, immunoreactivity for anti-GAβ antibody. By contrast, in the brain of the DM-affected adult monkey, we observed several neurons immunopositive for anti-GAβ antibody. Scale bars, 100 μm. (C) Quantitative image analysis of GAb-immunopositive area in the sections obtained from female normal adult monkey and DM-affected adult monkey brains. Data obtained from normal adult monkey brains were set as standards. Y-axes show the mean values of the quantified data. Values are means ± SD. *P < 0.02. (D) Dot blots showing the amount of GAβ generated in brains of cynomolgus monkeys of different ages. The blot samples were adjusted to 1 μg, 2.5 μg, or 5 μg of total protein. Dot blot analyses showed that GAβ generation increased in an age-dependent manner. (E) Dot blots showing the amount of GAβ generated in the brains of normal adult monkeys and DM-affected adult monkeys. The blot samples were adjusted to 1 μg, 2.5 μg, or 5 μg of total protein. The amount of GAβ in brains samples from DM-affected monkeys was significantly increased compared to those from normal adult monkeys. CT, normal adult monkeys; DM, DM-affected adult monkeys.

doi:10.1371/journal.pone.0117362.g004

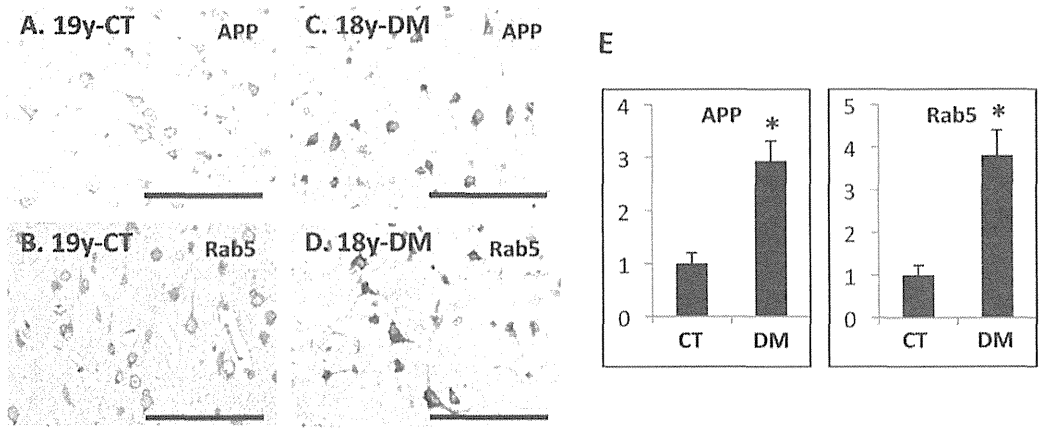

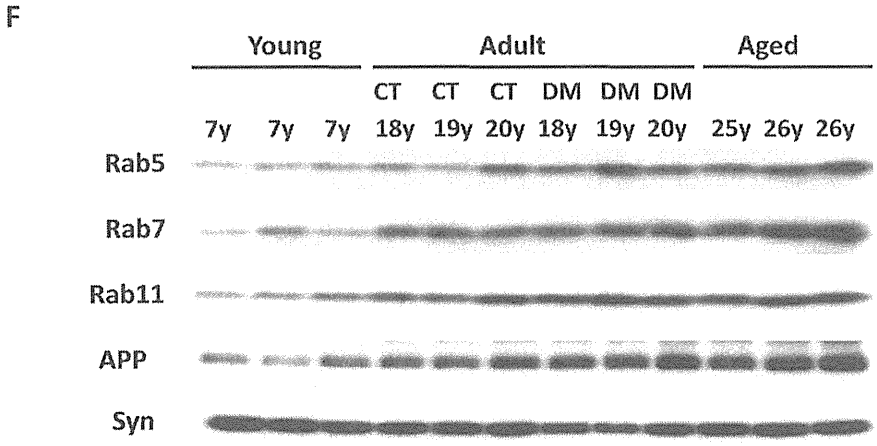

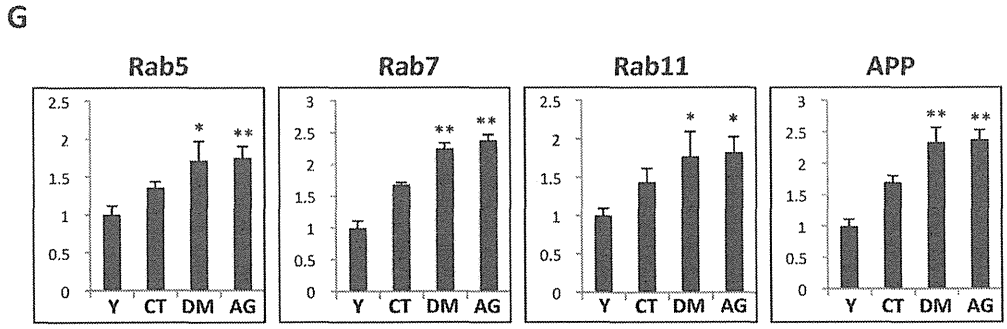

Fig 5. Immunohistochemistry and Western blot analyses of Rab5, Rab7, Rab11, and APP in the brains of normal and DM-affected monkeys. Images of temporal lobe sections from a 19-year-old normal cynomolgus monkey (A, B) and an 18-year-old cynomolgus monkey with DM (C, D). Sections were immunostained with anti-APP antibody (A, C) or anti-Rab5 antibody (B, D), and then counterstained with hematoxylin. Scale bars, 100 μm. In the brains of normal adult monkeys, APP and Rab5 were observed as small granules in neurons (A, B). By contrast in the brains of DM-affected adult monkeys, APP- and Rab5-immunopositive granules were enlarged, and APP and Rab5 immunoreactivity was significantly more robust (C, D). (E) Quantitative image analysis of APP or Rab5-immunopositive area in the sections obtained from female normal adult monkey and DM-affected adult monkey brains. Data obtained from normal adult monkey brains were set as standards respectively. Y-axes show the mean values of the quantified data. Values are means ± SD. *$P < 0.01$. (F) Western blots showing the amounts of APP, Rab5, Rab7, Rab11, and synaptophysin in the brains of normal monkeys and DM-affected monkeys of different ages. Western blot analyses showed that APP and Rab GTPases were significantly increased in both DM-affected adult and aged monkey brains. In the brains of DM-affected adult monkeys, APP and Rab GTPases levels were obviously increased compared to those of normal adult monkeys. Lanes contained microsome fractions derived from the brains of young monkeys, normal adult monkeys, DM-affected adult monkeys, and aged

monkeys. CT, normal adult monkeys; DM, DM-affected adult monkeys. (G) Age-related and DM-related changes in APP, Rab5, Rab7, and Rab11 in cynomolgus monkey brains. Data obtained from young monkey brains were set as standards; *P<0.05 **P<0.01. Y-axes show the mean values of the quantified data. Y, young monkeys; CT, normal adult monkeys; DM, DM-affected adult monkeys; AG, normal aged monkeys.

doi:10.1371/journal.pone.0117362.g005

studies are needed, these findings suggest that DM can induce not only parenchymal Aβ pathology but also vascular Aβ pathology in an age-dependent manner.

To clarify the mechanism of how DM enhances Aβ pathology in the brain, we also assessed the amount of Aβ and GAβ, a seed molecule for Aβ aggregation [32]. Intriguingly, Aβ level was not so much increased in DM-affected adult monkey brains, in contrast to aged monkey brains (Fig. 4A). In DM-affected adult monkey brains, SP depositions were quite small quantities (Fig. 2I), and a couple of more years can induce age-dependent SP depositions in normal adult monkey brains [26, 36]. That may be why we could not find the significant increase of Aβ level between DM-affected adult monkey and normal adult monkey brains. On the other hand, both immunohistochemical and dot blot analyses demonstrated that the amount of GAβ was clearly increased in the brains of DM-affected adult monkeys compared to control adult monkey brains (Fig. 4B-E). These findings strongly suggest that the acceleration of GAβ generation might be responsible for the early deposition of SPs in the brains of DM-affected adult

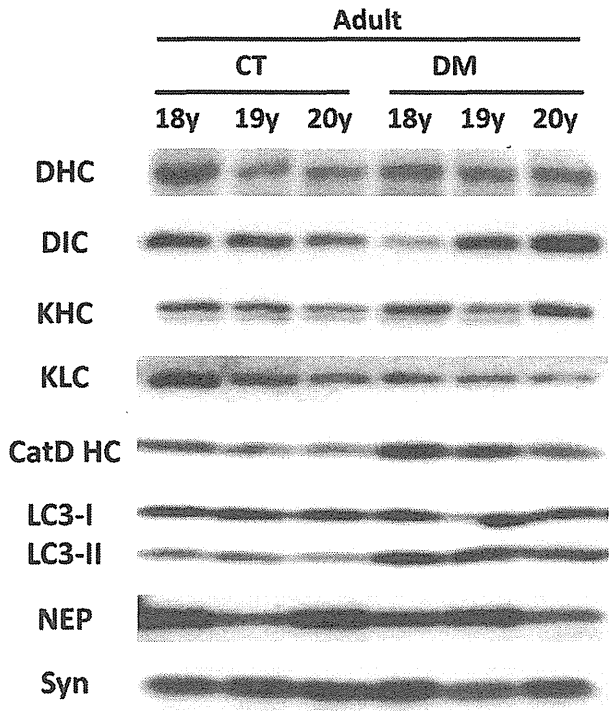

Fig 6. Western blot analyses of axonal motor proteins, cathepsin D heavy chain, autophagosome marker LC3, and neprilysin in the brains of normal and DM-affected adult monkeys. Western blots showing the amounts of axonal motor proteins, cathepsin D heavy chain (CatD HC), autophagosome marker LC3, and neprilysin (NEP) in the brains of normal and DM-affected adult monkeys. Western blot analyses showed that the level of axonal motor proteins such as dynein heavy chain (DHC), dynein intermediate chain (DIC), kinesin heavy chain (KHC), and kinesin light chain (KLC) unchanged. The level of CatD HC increased in DM-affected monkey brains, and LC3-II showed significant increase in DM-affected adult monkeys. We did not observed DM-related changes in LC3-I and neprilysin (NEP) level. CT, normal adult monkeys; DM, DM-affected adult monkeys.

doi:10.1371/journal.pone.0117362.g006

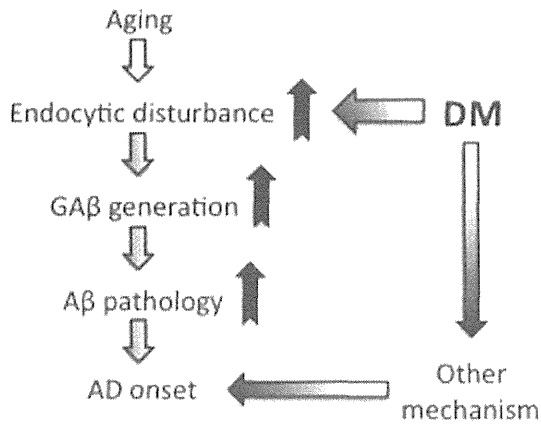

Fig 7. Hypothetical schema of DM-induced Aβ pathology leading to AD onset. From the results of this study, we propose that DM induces GAβ generation by exacerbating age-dependent endocytic disturbance, resulting in enhanced Aβ pathology in the brain. Although additional studies are needed to clarify the whole mechanisms underlying DM-associated pathology, we hypothesize that, at the very least, enhanced Aβ pathology accompanied by endocytic disturbance might be involved in the development of AD.

doi:10.1371/journal.pone.0117362.g007

monkeys. Moreover, the result of this study also suggests that enhanced Aβ aggregation could induce SP deposition without significant changes in total Aβ level. Relevant to proposed AD pathophysiogical mechanisms, we also observed apparent endocytic pathology, including enlarged early endosomes and APP accumulation in neurons of DM-affected adult monkeys (Fig. 5A-E). Western blot analyses confirmed a significant increase of Rab GTPases in these brains at nearly the same level as in aged monkey brains (Fig. 5F, G). Our previous studies showed that an increase in Rab GTPases is a good indicator for alterations in intracellular endosome trafficking associated with a particular Rab GTPase [45, 46]. Indeed, increased Rab GTPase levels are strongly associated with endocytic disturbance [45, 46]. The observation that experimentally induced disorders of the endocytic pathway cause GAβ-dependent Aβ pathology [34, 52] supports the premise that endocytic disturbance is likely responsible for enhanced GAβ generation. Along these lines, we surmise that intracellular endosome trafficking would be altered in the brains of DM-affected adult monkeys, resulting in severe endocytic disturbance, as observed in aged monkey brains. This might be why GAβ generation was enhanced, thereby inducing SP deposition (Fig. 2). Moreover, the results of this study strongly support the idea that endocytic disturbance is essentially involved in the development of AD pathology [33, 34, 42–45].

A recent study showed that the expression of axonal transport motor proteins was altered in experimentally DM-induced rodent model, and axonal transport motor proteins are indeed required for endosome trafficking [48, 49]. However, in the present study, we did not find any changes in axonal motor protein levels, suggesting that the mechanism underlying endocytic disturbance in the brains of DM-affected adult monkeys would be independent of axonal motor protein levels. Previous finding showed that the breakdown in lysosomal degradation also induces endocytic disturbance [50]. In DM-affected adult monkey brains, the level of CatD heavy chain increased in DM-affected adult monkey brains, indicating that the endosomal-lysosomal system is activated as such in AD patient brains (Fig. 6) [53]. This finding suggests that DM really enhances AD pathology. On the other hand, we observed the significant increase in autophagosome marker LC3-II level in DM-affected adult monkey brains (Fig. 6). Since LC3-I level was unchanged, the induction of autophagy was not altered, but lysosomal-